Pol. J. Environ. Stud. Vol. XX, No. X (XXXX), 1-15
DOI: 10.15244/pjoes/195371 ONLINE PUBLICATION DATE:

Original Research

Hydrochemical Characteristics and Formation Mechanisms of an Antimony Mining Activity Area in the Upstream Water Source of Danjiangkou Reservoir, China

Hao Zhao[1,2]*, Lilei Zhao[1,2], Xiaoming Li[1], Zhirui Wang[1,2], Jianwei Sun[1,2], Hong Zhang[1]

[1]Xi'an Center of Mineral Resources Survey, China Geological Survey, Xi'an 710100, China
[2]Qinling-Loess Plateau Transition Zone Observation and Research Station for Coupling of Soil and Water Elements and Conservation of Biological Resources, Tongguan 714300, China

Received: 7 July 2024
Accepted:28 October 2024

Abstract

Antimony (Sb) is a major environmental pollutant that is widely present in nature and possesses toxicity and potential carcinogenicity. The mining of antimony ore can affect the quality of the water environment and the safety of drinking water for residents in the area. Taking the Gaolinggou antimony mining area in the Danjiangkou water source for the Middle Route of South-to-North Water Diversion Project (MRSNWDP) in China as the research object, systematic hydrochemical samples and hydrogen and oxygen isotope samples were collected for comprehensive hydrogeochemical analysis. The results show that: (1) The pH range of surface water in the study area is 3.09-8.30, with a mean of 7.21, indicating an overall neutral condition, while some local areas are acidic. The range of TH is 243.00-439.00 mg/L, with a mean of 314.69 mg/L. The TDS ranges from 262.00 to 598.00 mg/L, averaging at 384.38 mg/L. The dominant cations are Ca^{2+} and Mg^{2+}, while the dominant anions are HCO_3^- and SO_4^{2-}. The hydrochemical types vary frequently in space, including $HCO_3 \cdot SO_4$-Ca·Mg, $SO_4 \cdot HCO_3$-Ca·Mg, HCO_3-Ca·Mg, and SO_4-Ca·Mg. For groundwater, the mean pH is 7.52, with TH and TDS ranging from 269.00-542.00 mg/L and 291.00-652.00 mg/L, respectively, averaging at 426.67 mg/L and 504.67 mg/L, both slightly higher than those of surface water. The dominant cations and anions are Ca^{2+} and HCO_3^-, respectively, with hydrochemical types mainly HCO_3-Ca·Mg and $HCO_3 \cdot SO_4$-Ca·Mg. The mine water has a pH value of 8.03, indicating a weakly alkaline condition with the highest TDS content. It is rich in SO_4^{2-}, Ca^{2+}, and Mg^{2+}, and the hydrochemical type is $SO_4 \cdot HCO_3$-Ca·Mg. (2) The hydrochemical characteristics in the study area are primarily controlled by rock weathering, with carbonate and silicate weathering and dissolution as the main processes. Positive cation exchange occurs in the water bodies. Surface water is significantly affected by mining activities, while groundwater is influenced

*e-mail: zhaohao1990@126.com
Tel.: +0086-180-826-288-52

by a combination of agricultural activities, domestic sewage, and mining activities. (3) In addition to atmospheric precipitation and dissolution of salt rocks, the excess Na^+ in the water bodies mainly originates from the dissolution of sodium-bearing silicates and the contribution of cation exchange processes. Ca^{2+} and Mg^{2+} mainly originate from the weathering of carbonate rocks dominated by calcite and the dissolution of gypsum. Carbonic acid and sulfuric acid both participate in the weathering and dissolution of carbonate rocks. So_4^{2-} and Cl^- are significantly influenced by mining activities. The antimony in surface water is primarily influenced by the mining of antimony ore, with the average concentration of antimony in the mining area being 6.4 times that of the mainstream of the Luohe River. Meanwhile, the antimony in groundwater mainly originates from the lateral recharge of surface water. The results can provide a reference for the water resource security assurance and rational development and utilization of the MRSNWDP.

Keywords: antimony mining activity area, hydrochemical characteristics, control factors, cation exchange, cluster analysis

Introduction

Antimony (Sb) is a widely occurring metalloid element in nature and an internationally recognized major environmental pollutant with toxicity and potential carcinogenicity [1-5]. Many countries and regions, including China, have listed it as a key pollutant for prevention and control [6] or one of the pollutants requiring priority treatment [7-9]. The abundance of Sb in the Earth's crust is approximately 0.2 ug/g, primarily existing in the forms of Sb-containing sulfides (Sb_2S_3) and oxides (Sb_2O_3). The Sb concentration in uncontaminated water is less than 1 ug/L, and the Sb concentration in soil ranges from 0.3 to 8.6 ug/g [9-11]. Sb in soil and water environments is primarily influenced by geological backgrounds and human activities [12, 13]. The Sb flux changes on the Earth's surface caused by human activities far exceed the natural flux, accounting for 83% of the total flux, with mining activities being the primary anthropogenic source [14, 15]. Extensive research by scholars on heavy metal pollution in soil and water environments of typical antimony mining areas has revealed that the mining, smelting, and storage processes of antimony ore generate substantial pollutants, including waste slags and wastewater. Through oxidation, leaching, and other processes, antimony-bearing minerals release metallic Sb and SO_4^{2-} into freshwater systems, significantly elevating Sb concentrations in the water environment. This phenomenon has been observed in antimony mining areas in various locations, such as Australia [16], Albania [17], Iran [18], South Korea [19], and Hunan, Guizhou, Guangxi, Yunnan, and Shaanxi provinces in China [20-25]. Antimony mining areas, being the most severely contaminated and affected by environmental Sb pollution, pose significant challenges to the water safety of local residents due to their contaminated water environments. Consequently, a profound understanding of the hydrochemical characteristics and formation mechanisms in antimony mining areas is vital for improving regional water environmental quality and mitigating water-related environmental risks.

The formation and evolution of hydrochemical components in water bodies are influenced by a combination of factors, including geological structures, stratigraphic lithology, climate, and human activities [26–28]. Understanding these processes is a key approach to studying regional water quality. Currently, based on the theories of hydrogeology and hydrogeochemistry, scholars systematically analyze the hydrochemical characteristics, influencing factors, and main ion sources of different water bodies using multivariate statistical methods such as mathematical statistics, Pearson correlation analysis, and hierarchical cluster analysis. They also employ tools like Piper's triangular diagram, Gibbs diagram, Na-endmember diagram, and ion ratio relationships [29–36], providing a vast array of theoretical knowledge and technical methodologies for identifying the sources and evolution patterns of regional hydrochemical components and indicating the processes of water-rock interactions.

The study area is located upstream of the Danjiang River Basin, which is the main water conservation area for the Middle Route of the South-to-North Water Diversion Project (MRSNWDP). The area is rich in mineral resources, and long-term mineral resource development has resulted in the disorderly stacking of a large amount of waste residue, leading to prominent phenomena of slag seepage, water inrush from mines, and water quality in some tributary rivers exceeding standards. In 2021, heavy rainfall caused multiple cases of abnormal antimony concentrations in the Danjiang River Basin. These primarily involved the Caiwa Antimony Mine in Danfeng County, the Gaolinggou Antimony Mine in Shangzhou District, and the Luoyugou Antimony Mine in Shanyang County, posing significant environmental risks to the water quality of the basin. Therefore, this paper selects the Gaolinggou Antimony Mine active area as the research object. Based on the identification of regional hydrogeological conditions, it explores the hydrogeochemical characteristics and formation mechanisms using hydrochemical and hydrogen-oxygen isotope data, aiming to provide a scientific basis for ensuring water

safety and the rational development and utilization of the MRSNWDP.

Study Area

The antimony mining activity area of Gaolinggou is administratively part of Shangzhou District, Shangluo City, Shaanxi Province, China. The region is characterized by continuous mountain ranges and crisscrossing valleys, with a semi-humid monsoon climate located at the southern fringe of the warm temperate zone. The annual average temperature is 12.8°C, with the lowest temperature reaching -14.8°C and the highest temperature soaring to 40.7°C. The multi-year average precipitation is 694.5 mm, mainly concentrated from July to September, resulting in uneven rainfall distribution throughout the year. The multi-year average evaporation is 1300.1 mm. The terrain within the mining area is generally higher in the southeast and lower in the northwest, characterized by complex landforms and well-developed valleys. It belongs to the medium-low mountainous landform structure on the southern slope of the East Qinling Mountains. The water system in the area belongs to the Danjiang tributary of the Yangtze River system, with the main river being the Luo River on the west side. Other secondary valleys are developed, all of which are first- or second-order tributaries of the Luo River, spreading in a dendritic pattern. The tributaries flow into Gaolinggou along valleys such as Yangpogou, Zhaogou, and Chengchuigou, and then converge into the Luo River from east to west, eventually joining the Danjiang River near Changchuan New Village (Fig. 1).

The tectonic location of the study area is in the Caledonian fold belt of the East Qinling Fold System in the Qinqi geosyncline, north of the Shangdan major fault. The regional strata are deeply metamorphosed with complex folds and faults. The exposed strata in the area mainly include the Lower Proterozoic Qinling Group (Pt_1qn^2) graphite-bearing marble with gneiss, Upper Triassic (T_3) carbonaceous silty slate with sandstone, Tertiary (E) sandstone and glutenite, and Quaternary (Q) gravel and sandy loam [37, 38]. The main metallic mineral is stibnite; secondary minerals include pyrite, antimonite, yellow stibnite, red stibnite, and galena; gangue minerals include quartz, dolomite, calcite, barite, graphite, and sericite [39]. The types of groundwater in the area can be divided into four categories based on occurrence conditions: (1) Loose rock pore water, mainly distributed in river valleys, floodplains, and terraces on both sides, with a small distribution range. The aquifer is mainly composed of Quaternary residual slope deposits and alluvial-diluvial deposits, consisting of rock debris, gravel, sand, and clay, with a thickness of 1-2m. It is permeable but water-bearing, and weakly water-rich. (2) Clastic rock pore-fissure water, distributed in the southern part of

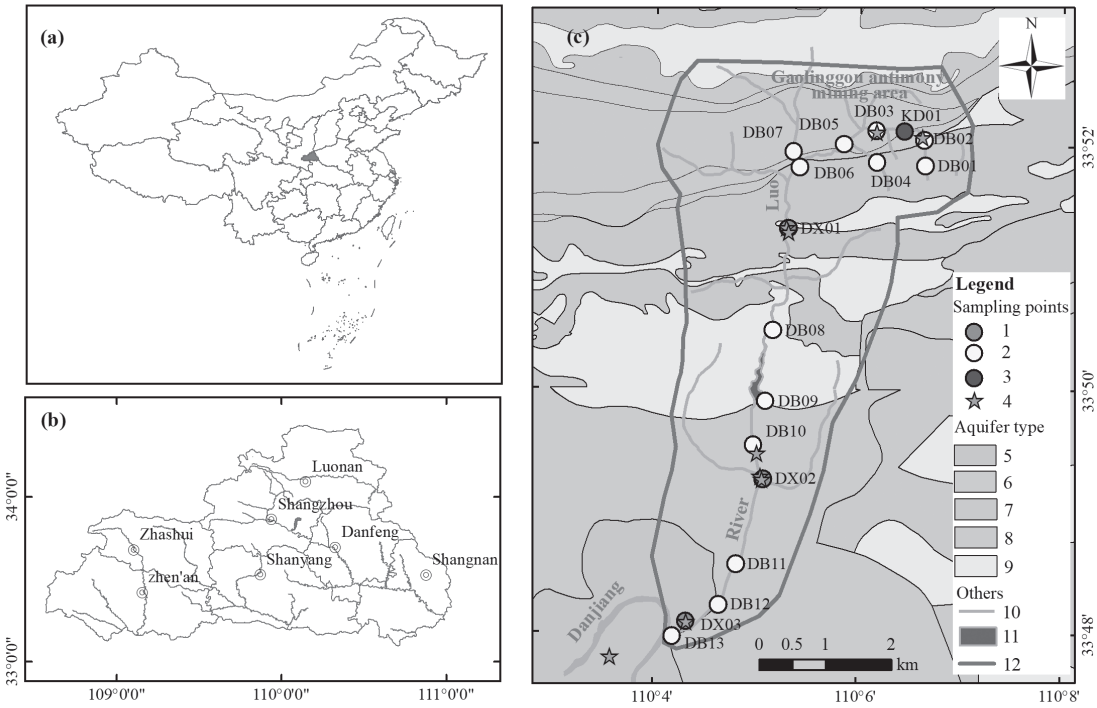

1-Groundwater, 2-Surface water, 3-Mine water, 4-Hydrogen and oxygen isotopes, 5-Loose rock pore water, 6-Clastic rock pore-fissure water, 7-Carbonate rock fissure-karst water, 8-Metamorphic rock fissure water, 9-Magmatic rock fissure water, 10-River, 11-Reservoir, 12-Study area.

Fig. 1. Geographical location and distribution of sampling points in the study area. (a) China's national geographical boundaries, with the red section indicating the relative location of Shangluo City, which is located in the upstream water source area of the Danjiangkou Reservoir, within China; (b) The administrative geographical boundaries of Shangluo City, with the red area indicating the study area; (c) Simplified hydrogeological map of the study area and sampling point locations.

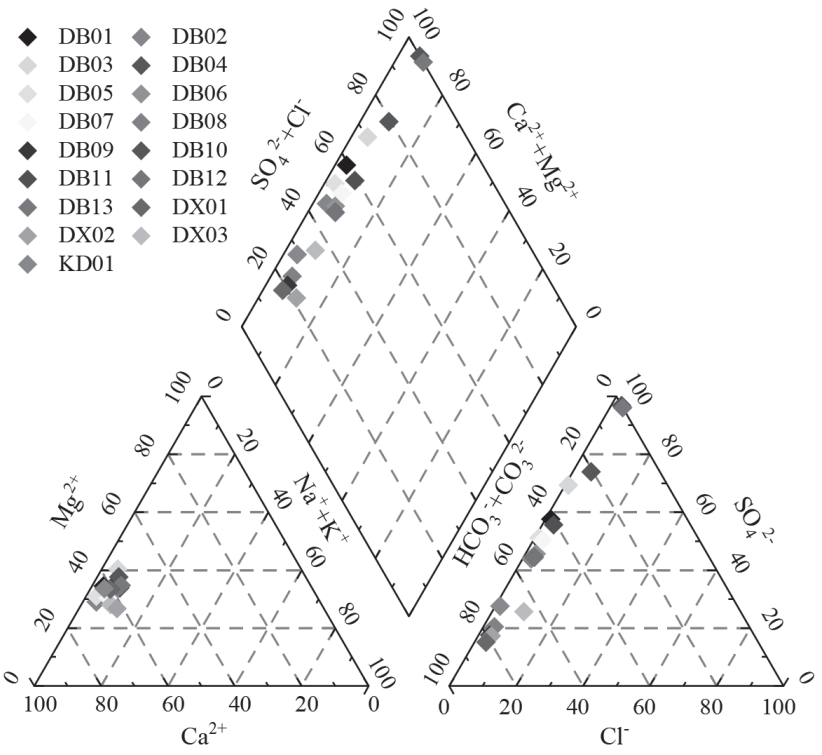

Fig. 2. Piper diagram of the major ions in the study area.

the study area, with Tertiary sandstone and glutenite as the lithology, and weakly water-rich. (3) Carbonate rock fissure-karst water, widely distributed in the area, with marble and graphite marble as the main lithology. The rocks are hard, medium-thick layered, structurally intact, with underdeveloped fissure-karst, and generally weakly water-rich. (4) Bedrock fissure water, which can be divided into metamorphic rock fissure water and magmatic rock fissure water according to lithology, structure, and geomorphic conditions. Metamorphic rock fissure water is mainly distributed in the northern part of the work area, with gray carbonaceous silty slate with glutenite, two-mica gneiss, and biotite plagioclase gneiss as the main lithology of the aquifer. The rock fissures are relatively developed, with dripping phenomena near fault zones or lithological boundaries, and generally weakly water-rich. Magmatic rock fissure water is distributed in the central part of the work area, with a small distribution range. The main lithology of the aquifer is plagioclase granite porphyry and medium-coarse-grained granite. The rocks of this aquifer are hard, structurally intact, with underdeveloped fissures, and generally weakly water-rich. Groundwater in the area is mainly replenished by atmospheric precipitation, flowing from high to low towards valleys and downstream, forming surface water in valleys.

Materials and Methods

Sample Collection and Analysis

In October 2023, a total of 13 surface water samples (DB01-DB13), 3 groundwater samples (DX01-DX03), and 1 mine water sample (KD01) were collected within the study area, spanning from the upstream Gaolinggou antimony mining area to the entrance to the Danjiang River of the Luo River. Among these samples, DB03 represents surface water that has undergone treatment at a wastewater treatment station, while DB10 and DB13 are surface water samples collected downstream of two separate emergency response sites. Furthermore, a total of 9 hydrogen and oxygen isotope samples were collected, comprising 3 samples from surface water, 3 samples from groundwater, 2 samples from atmospheric precipitation, and 1 sample from mine water (Fig. 1). Sample collection adhered to the "Technical Specifications for Environmental Monitoring of Groundwater" (HJ/T 146-2020). Water quality analysis samples were collected and stored in polyethylene plastic bottles (5 L), with the bottles and lids rinsed multiple times before sampling. Hydrogen and oxygen isotope samples were collected using brown glass vials (10 ml), with syringes and filters employed for the process. Immediately after sampling, labels were affixed to the containers, clearly indicating sampling time, sample number, and other relevant information.

The water quality analysis encompassed a range of inorganic indicators, including pH, total hardness (TH),

Table 1. Statistics of hydrochemical parameters of surface water, groundwater, and mine water in the study area.

Samples	Index	pH	TH	TDS	K^+	Na^+	Ca^+	Mg^+	Cl^-	SO_4^{2-}	HCO_3^-	NO_3^-
Surface Water n=13	Maximum	8.30	439.00	598.00	2.16	17.50	119.00	39.40	18.60	339.00	405.00	10.20
	Minimum	3.09	243.00	262.00	1.29	5.37	59.60	22.00	4.00	28.10	0.00	3.21
	Average	7.21	314.69	384.38	1.58	8.85	82.36	27.23	7.12	162.10	191.38	7.70
	CV/%	24.77	22.63	25.26	17.56	35.20	27.94	22.37	51.62	61.79	58.38	26.14
Groundwater n=3	Maximum	7.72	542.00	652.00	2.96	25.70	150.00	40.50	36.30	132.00	464.00	70.90
	Minimum	7.41	269.00	291.00	1.59	6.94	69.20	23.20	6.60	39.40	270.00	8.67
	Average	7.52	426.67	504.67	2.46	18.31	116.73	32.70	18.80	84.00	386.00	45.02
	CV/%	2.34	33.13	37.53	30.74	54.58	36.19	26.83	82.68	55.23	26.54	71.99
Mine Water n=1	/	8.03	698.00	899.00	3.02	14.40	161.00	71.60	5.30	492.00	267.00	1.94

Note: pH is dimensionless; the unit for other ion mass concentrations is mg/L.

total dissolved solids (TDS), as well as specific ions such as K^+, Na^+, Ca^{2+}, Mg^{2+}, Cl^-, SO_4^{2-}, HCO_3^-, and NO_3^-. The pH and TDS were measured on-site using an AQUA TROLL 400 portable multi-parameter water quality analyzer. The remaining indicators were analyzed by Shaanxi Geological and Mineral Experimental Research Institute Co., Ltd. (Xi'an Mineral Resources Testing Center of the Ministry of Natural Resources). For TH, an electronic balance and burette were used for the determination. The cations K^+, Na^+, Ca^{2+}, and Mg^{2+} were measured using an Agilent 5110 Inductively Coupled Plasma Optical Emission Spectrometer (ICP-OES). The anions Cl^-, SO_4^{2-}, and NO_3^- were analyzed with an ICS1100 Ion Chromatograph. HCO_3^- was determined through titration using a burette. The hydrogen and oxygen isotope samples were analyzed by the Analytical and Testing Research Center of Beijing Research Institute of Uranium Geology, adhering to the analytical methods for ^2H and ^{18}O outlined in the "Methods for Groundwater Analysis" (DZ/T 0064-2021). The measurements were performed using a MAT-253 Gas Isotope Mass Spectrometer. The detection limits and test results for all indicators met the quality requirements, ensuring the accuracy and reliability of the data obtained.

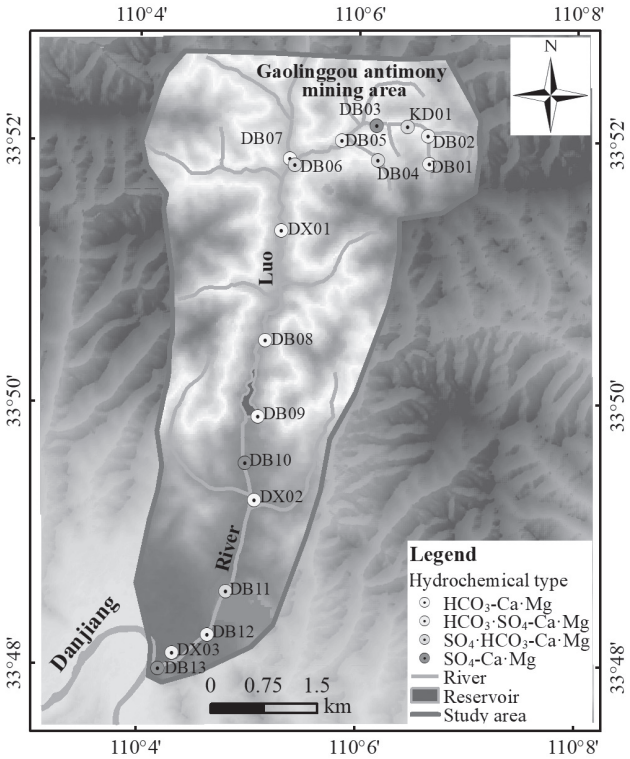

Fig. 3. Spatial distribution of hydrochemical types in the study area.

Data Analysis Methods

SPSS 27 software was used to perform mathematical statistics, Pearson correlation analysis, and cluster analysis on the hydrochemical data. Origin 2021 and ArcGIS 10.5 software were used to create diagrams, including Piper trilinear diagrams, Gibbs diagrams, ion ratio diagrams, and spatial distribution maps of hydrochemical types.

Results and Discussion

Hydrochemical Characteristics

Characteristics of Hydrochemical Ion Composition

The statistical results of hydrochemical parameters in the study area are shown in Table 1. The results indicate that there are certain differences in hydrochemical parameters among different water bodies in the study area. The pH range of surface water is 3.09~8.30, with an average value of 7.21, indicating an overall neutral condition, but some individual samples show strong acidity. The TH ranges from 243.00 to 439.00 mg/L, with an average of 314.69 mg/L, indicating that the water is generally hard, while a few samples are slightly hard. The TDS range is 262.00~598.00 mg/L, with an average of 384.38 mg/L, classifying it as low-salinity freshwater. The dominant cations are Ca^{2+} and Mg^{2+}, with their respective mass concentrations in descending order: $Ca^{2+} > Mg^{2+} > Na^{+} > K^{+}$, with average values of 82.36 mg/L, 27.23 mg/L, 8.85 mg/L, and 1.58 mg/L, respectively. The dominant anions are HCO_3^- and SO_4^{2-}, and their mass concentrations follow the order: $HCO_3^- > SO_4^{2-} > NO_3^- > Cl^-$, with average values of 191.38 mg/L, 162.10 mg/L, 7.70 mg/L, and 7.12 mg/L, respectively. The coefficients of variation (CV) for SO_4^{2-}, HCO_3^-, and Cl^- in surface water are relatively high, at 61.79%, 58.38%, and 51.62%, respectively, indicating significant spatial variation and complex evolution of these ions.

The average pH of groundwater is 7.52, slightly higher than that of surface water. The TH and TDS ranges are 269.00~542.00 mg/L and 291.00~652.00 mg/L, respectively, with average values of 426.67 mg/L and 504.67 mg/L, both slightly higher than those of surface water. The dominant cations and anions in groundwater are also Ca^{2+} and HCO_3^-, respectively, with similar mass concentration orders as in surface water. The CVs for Cl^-, NO_3^-, SO_4^{2-}, and Na^+ in groundwater are relatively high, at 82.68%, 71.99%, 55.23%, and 54.58%, respectively, suggesting complex evolution processes that may be influenced by human activities such as agricultural production, domestic sewage discharge, and mining activities.

The pH of mine water is 8.03, indicating weak alkalinity. It has the highest TDS content, and its SO_4^{2-}, Ca^{2+}, and Mg^{2+} contents are higher than those in surface water and groundwater, possibly related to the oxidation of sulfur-bearing minerals and the dissolution of carbonate minerals in the study area.

Hydrochemical Types and Evolution

A Piper trilinear diagram was constructed using the percentage of milligram equivalents of major cations and anions to analyze the hydrochemical composition characteristics of different water samples [36] (Fig. 2). In the study area, the cations are primarily concentrated near the Ca^{2+} and Mg^{2+} endmembers, with a notable distance from the Na^+ and K^+ endmembers. Similarly, the anions are predominantly located near the HCO_3^- and SO_4^{2-} endmembers, maintaining a substantial distance from the Cl^- endmember.

The Shukaliev method was adopted to classify the hydrochemical types of different water bodies in the study area, and a spatial distribution map of hydrochemical types was plotted (Fig. 3). The results showed that the surface water in the study area had hydrochemical types of $HCO_3 \cdot SO_4$-Ca·Mg (4 groups), $SO_4 \cdot HCO_3$-Ca·Mg (3 groups), HCO_3-Ca·Mg (3 groups), and SO_4-Ca·Mg (3 groups); the groundwater had hydrochemical types of HCO_3-Ca·Mg (2 groups) and $HCO_3 \cdot SO_4$-Ca·Mg (1 group); and the mine water had a hydrochemical type of $SO_4 \cdot HCO_3$-Ca·Mg (1 group). According to the spatial distribution of hydrochemical types, the hydrochemical types of the Gaolinggou antimony mining area were $HCO_3 \cdot SO_4$-Ca·Mg (DB01, DB02, DB05), $SO_4 \cdot HCO_3$-Ca·Mg (DB04, DB06), and SO_4-Ca·Mg(DB03). The changes in hydrochemical types were controlled by the increase in SO_4^{2-} content, which might be related to the influx of mine water and leachate with high SO_4^{2-} content, as well as the addition of polyferric sulfate as a treatment agent at the wastewater treatment station. The surface water of the Luo River exhibited a hydrochemical type of HCO_3-Ca·Mg (DB07, DB08, DB09) above Emergency Response Point 1(DB10), which evolved sequentially downstream to SO_4-Ca·Mg (DB10), $SO_4 \cdot HCO_3$-Ca·Mg (DB11), $HCO_3 \cdot SO_4$-Ca·Mg (DB12), and SO_4-Ca·Mg (Emergency Response Point 2, DB13) below Emergency Response Point 1. The hydrochemical types were jointly controlled by the initial significant increase and subsequent gradual decrease in SO_4^{2-} content and the initial rapid decrease and subsequent gradual increase in HCO_3^- content, indicating that the emergency acidification treatment had a significant impact on the rapid changes in the hydrochemical types of surface water. Additionally, the hydrochemical type of groundwater evolved from HCO_3-Ca·Mg (DX01, DX02) to $HCO_3 \cdot SO_4$-Ca·Mg (DX03), suggesting that the surface water downstream of the Luo River also had a certain impact on the groundwater.

Correlation Analysis

Pearson correlation analysis [31] and cluster analysis [32] were used to jointly reveal the correlation of hydrochemical components, and to preliminarily judge

Table 2. Correlation coefficient of Hydrochemical Composition of surface water in the study area.

Index	pH	TH	TDS	K^+	Na^+	Ca^{2+}	Mg^{2+}	Cl^-	SO_4^{2-}	HCO_3^-
pH	1									
TH	0.222	1								
TDS	-0.249	0.848**	1							
K^+	0.087	0.770**	0.663*	1						
Na^+	-0.124	0.258	0.501	0.441	1					
Ca^{2+}	0.346	0.968**	0.718**	0.751**	0.133	1				
Mg^{2+}	0.119	0.905**	0.773**	0.910**	0.363	0.889**	1			
Cl^-	-0.236	0.374	0.636*	0.463	0.904**	0.200	0.430	1		
SO_4^{2-}	-0.675*	0.436	0.838**	0.336	0.541	0.270	0.423	0.653*	1	
HCO_3^-	0.803**	0.326	-0.216	0.313	-0.390	0.500	0.343	-0.439	-0.679*	1

Note: *At the level of 0.05 (two tails), the correlation is significant; ** at the level of 0.01 (two tails), the correlation is significant.

whether each ion (or sampling point) had the same material source, reflecting its hydrogeochemical process. Since there are few underground water samples and mine water samples, only surface water chemistry was analyzed. The Pearson correlation coefficients indicate (Table 2) that: pH in the surface water is significantly positively correlated with HCO_3^- ($p<0.01$), and negatively correlated with SO_4^{2-} ($p<0.05$), with correlation coefficients of 0.803 and -0.675 respectively; TH was positively correlated with Ca^{2+}, Mg^{2+}, K^+($p<0.01$), and the correlation coefficients were 0.968, 0.905, 0.770, respectively; TDS was significantly correlated with SO_4^{2-}, Mg^{2+}, Ca^{2+}, K^+, Cl^-, and negatively correlated with HCO_3^-, indicating that the main contribution of TDS in surface water came from SO_4^{2-}, Mg^{2+}, and Ca^{2+}. Ca^{2+}, $Mg^{2+}$and K^+ were significantly correlated, while Na^+ and Cl^- were significantly correlated, indicating they may have the same source.

The R-mode cluster analysis (Fig. 4a) grouped the hydrochemical indicators into three clusters: Cluster 1 includes K^+, Mg^{2+}, Ca^{2+}, and TH; Cluster 2 comprises Na^+, Cl^-, SO_4^{2-}, and TDS; Cluster 3 consists of pH and HCO_3^-. The clustering results of hydrochemical indicators are consistent with the Pearson correlation analysis. The Q-mode cluster analysis (Fig. 4b) grouped the sampling points into four clusters: Cluster 1 includes DB13 and DB10; Cluster 2 comprises DB03; Cluster 3 includes DB07, DB08, DB09, DB11, and DB12; Cluster 4 includes DB01, DB02, DB04, DB05, and DB06. From the spatial distribution of sampling points and hydrochemical characteristics, it can be inferred that: Cluster 1 (DB13 and DB10) represents two emergency response points downstream of the Luo River; Cluster 2 (DB03) is the antimony-containing wastewater treatment station in Gaolinggou, where the addition of polyferric sulfate treatment agent led to an increase in SO_4^{2-} concentration and a significant decrease in

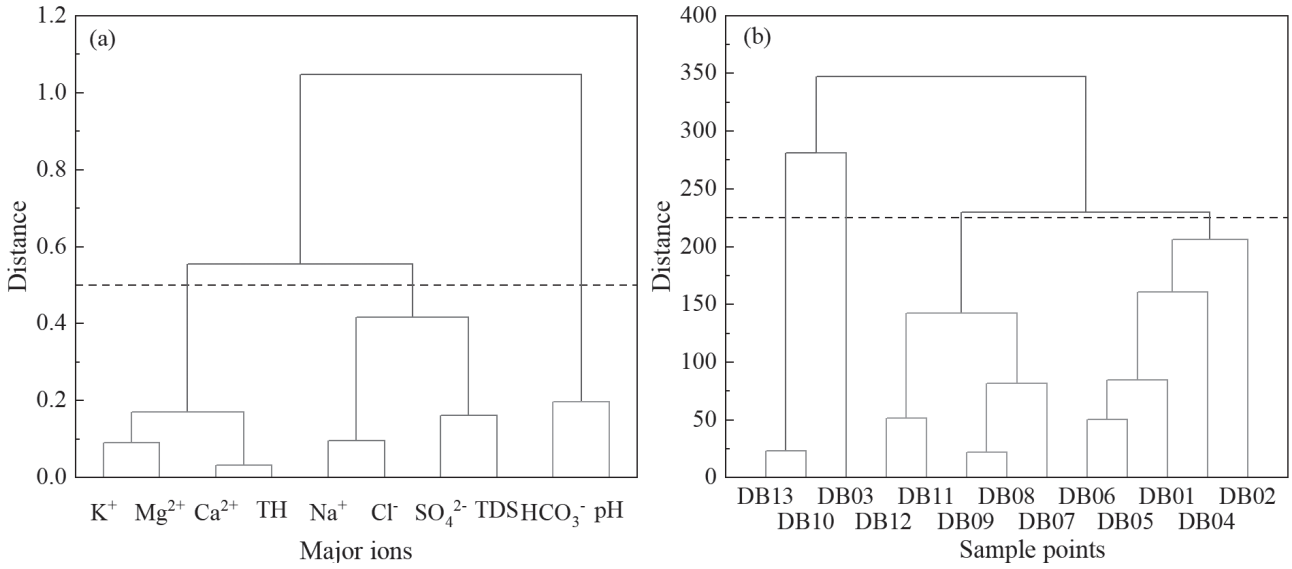

Fig. 4. Cluster analysis of R-type (a) and Q-type (b) hydrochemical indexes of surface water.

HCO_3^- concentration, indicating the direct impact of mining activities on the surface water environment; Cluster 3 is mainly distributed in the mainstream of the Luo River, while Cluster 4 is mainly distributed in Gaolinggou, indicating the surface water environmental characteristics of the mainstream of the Luo River and the antimony mining area in Gaolinggou, respectively.

Influencing Factors of Hydrochemistry

Rock Weathering

The Gibbs diagram is often used to analyze the hydrochemical evolution process of different water bodies and determine the influence degree of atmospheric precipitation, rock weathering, and evaporation-concentration on the main ion sources of water bodies [34, 35]. The TDS variation ranges of surface water and groundwater in the study area are 262.00~598.00mg/L and 291.00~652.00mg/L, respectively; the concentration ratios of $Na^+/(Na^+{+}Ca^{2+})$ are 0.04~0.14 and 0.09~0.16, respectively; the concentration ratios of $Cl^-/(Cl^-{+}HCO_3^-)$ are 0.01~1.00 and 0.02~0.08, respectively. The TDS of the mine water is 899.00mg/L, the concentration ratio of $Na^+/(Na^+{+}Ca^{2+})$ is 0.08, and the concentration ratio of $Cl^-/(Cl^-{+}HCO_3^-)$ is 0.02. As shown in Fig. 5, most water samples fall in the middle-left area of the Gibbs diagram, indicating that the hydrochemical components in the study area are mainly controlled by rock weathering, with relatively small atmospheric precipitation and evaporation-concentration effects. However, some surface water samples (DB10, DB13) still fall outside the dotted line of the control area, mainly due to the acidity of the water body at this point, the absence of HCO_3^- in surface water, and the proximity of the sample points to the emergency response point downstream of the Luo River, which is greatly affected by human activities.

The Gaillardet model is adopted to further reflect the leaching source of hydrochemical components during rock weathering [40, 41]. As shown in Fig. 6, the concentration ratios among Mg^{2+}/Na^+, HCO_3^-/Na^+, and Ca^{2+}/Na^+ indicate that after eliminating the impact of acid treatment at the two emergency response points DB10 and DB13 (where HCO_3^- was not detected), the sampling points of different water bodies are mainly distributed between silicate rocks and carbonate rocks, and closer to the carbonate rock endmember. This suggests that the hydrochemical components in the study area are jointly influenced by the weathering and dissolution of carbonate rocks and silicate rocks, but the weathering contribution of carbonate rocks is greater.

Cation Exchange

Cation exchange is a natural phenomenon that participates in the hydrochemical evolution of water bodies and alters the composition of some ions during water-rock interactions, playing a significant role in the formation of hydrochemistry. Typically, the relationship between $(Na^+{+}K^+{-}Cl^-)$ and $(Ca^{2+}{+}Mg^{2+}{-}SO_4^{2-}{-}HCO_3^-)$ can indicate whether cation exchange occurs. Here, $(Na^+{+}K^+{-}Cl^-)$ represents the increase or decrease of Na^+ beyond salt rock dissolution, while $(Ca^{2+}{+}Mg^{2+}{-}SO_4^{2-}{-}HCO_3^-)$ represents the increase or decrease of Ca^{2+} and Mg^{2+} beyond calcite, dolomite, and gypsum [32, 33, 42]. As shown in Fig. 7a, the surface water sampling points are distributed along the line $y=-0.299x+0.227$ ($R^2=0.436$), and most of the surface water, groundwater, and mine water samples are located near the line $y=-x$, indicating that cation exchange occurs in the water bodies of the study area.

The chloro-alkali indices [43] (CAI-I and CAI-II) are employed to further determine the direction and intensity of cation exchange in water bodies. When both CAI-I and CAI-II are positive, Ca^{2+} and Mg^{2+} in the aquifer medium exchange Na^+ and K^+ from the water, resulting in reverse cation exchange. Conversely, when both CAI-I and CAI-II are negative, forward cation exchange occurs. The greater the absolute values of CAI-I and CAI-II, the stronger the cation exchange [44].

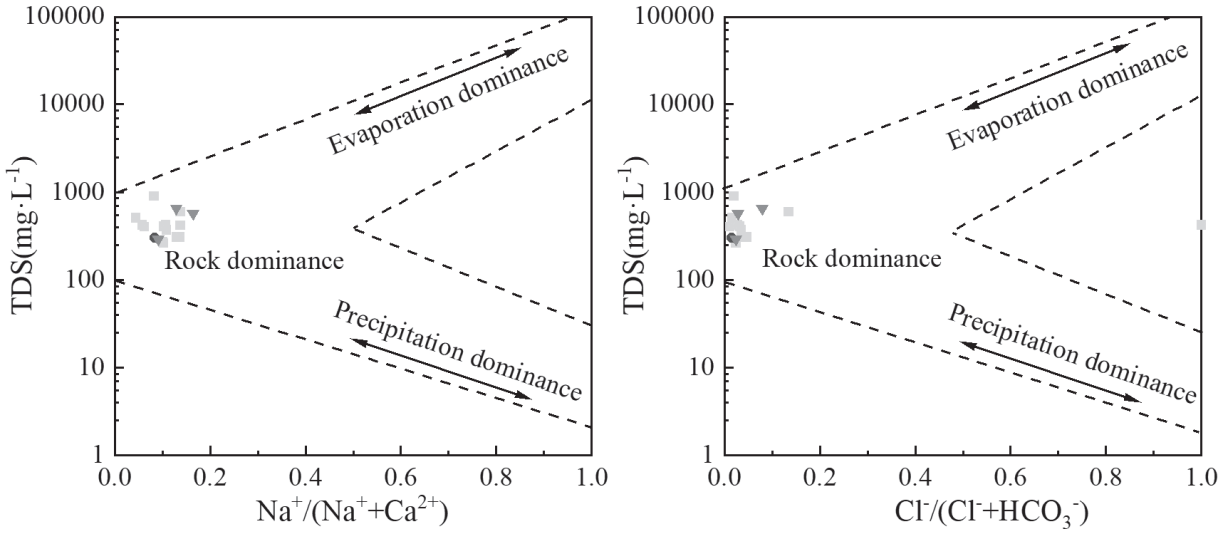

Fig. 5. Gibbs diagram of hydrochemical parameters in the study area.

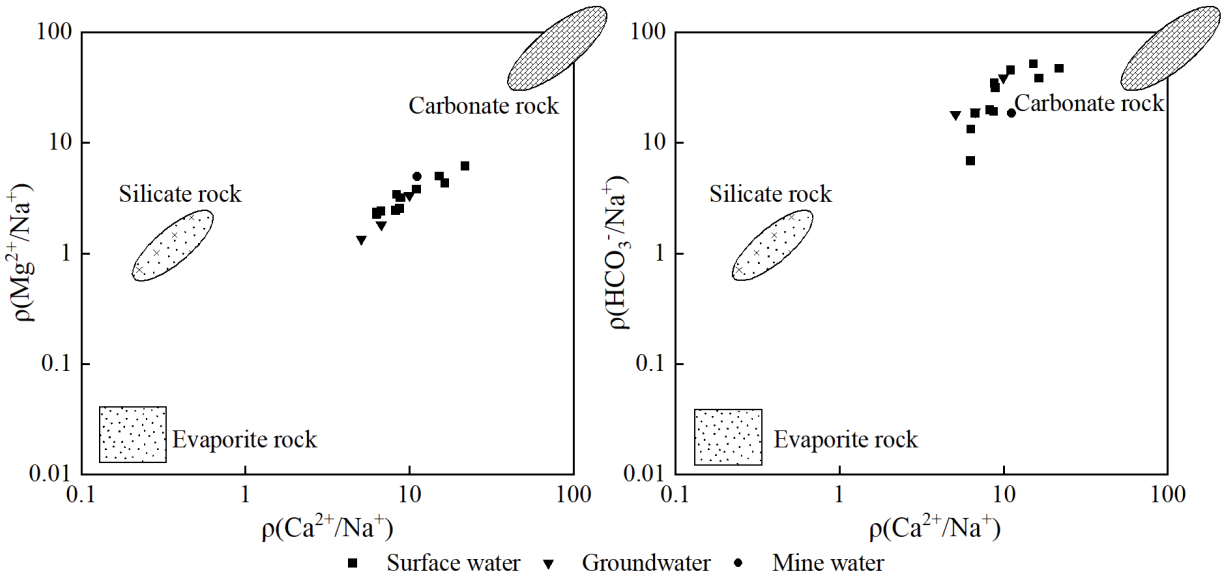

Fig. 6. The relationship of concentration ratio between Mg^{2+}/Na^+, HCO_3^-/Na^+ and Ca^{2+}/Na^+.

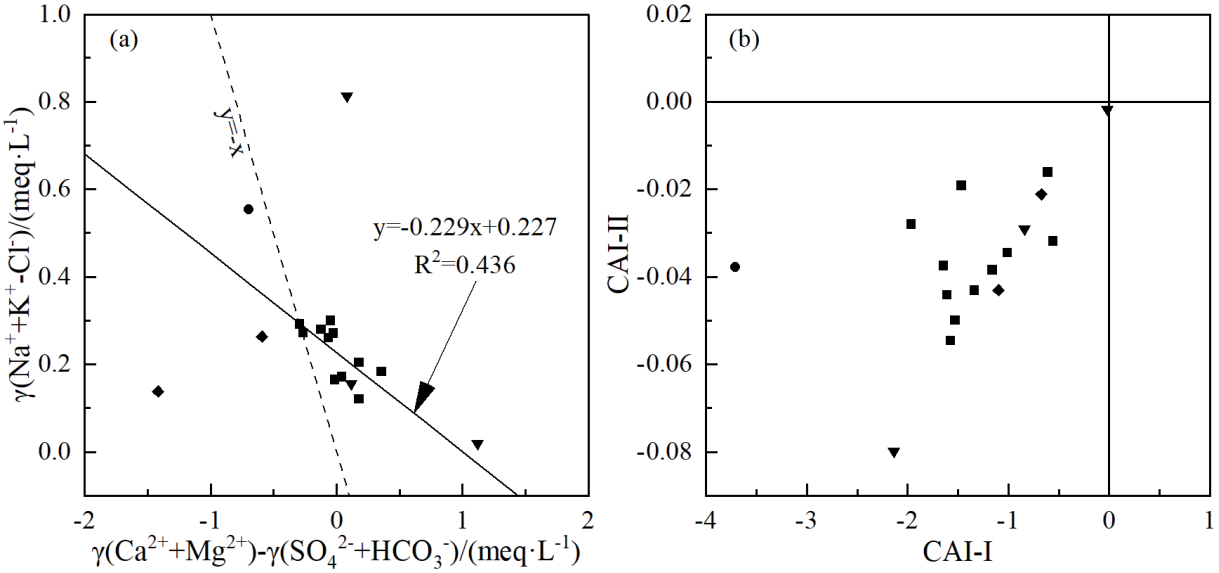

Fig. 7. Cation exchange (a) and chlor-alkali index (b) in the study area.

As shown in Fig. 7b, both CAI-I and CAI-II of surface water, groundwater, and mine water in the study area are negative, indicating that forward cation exchange occurs. In this process, Ca^{2+} and Mg^{2+} in the water bodies exchange with Na^+ and K^+ in the aquifer medium, leading to an increase in Na^+ and K^+ content in the water. The absolute values of CAI-I and CAI-II indicate that the intensity of cation exchange follows the order of mine water > surface water > groundwater, with a more pronounced difference in groundwater compared to surface water.

Evaporation

Evaporation plays a significant role in hydrochemical evolution, and the hydrogen and oxygen isotopic characteristics of water bodies can reveal the recharge sources and interconversion relationships among different water bodies [42, 45]. In the study area, the variation range of δD in atmospheric precipitation is -35.6‰ to -46.4‰, and that of $\delta^{18}O$ is -8.2‰ to -6.0‰; for surface water, the variation range of δD is -64.5‰ to -62.0‰, and that of $\delta^{18}O$ is -10.3‰ to -10.1‰; for groundwater, the variation range of δD is -65.4‰

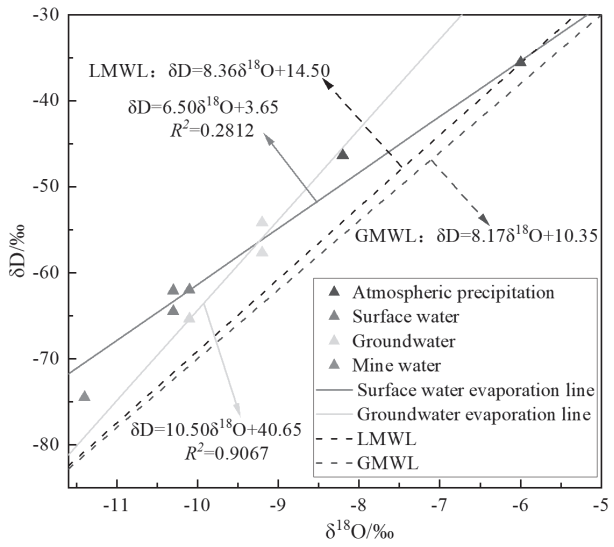

Fig. 8. δD versus $\delta^{18}O$ diagram in the study area.

to -54.2‰, and that of $\delta^{18}O$ is -10.1‰ to -9.2‰; the δD and $\delta^{18}O$ values of mine water are -74.5‰ and -11.4‰, respectively. The evaporation trend lines of hydrogen and oxygen isotopes for surface water and groundwater are $\delta D=6.50\delta^{18}O+3.65$(n=3, $R^2=0.2812$) and $\delta D=10.50\delta^{18}O+40.65$ (n=3, $R^2=0.9067$), respectively. The sample points fall above and to the left of the Global Meteoric Water Line (GMWL) [46] and the Local Meteoric Water Line (LMWL) for Shaanxi [47] (Fig. 8), indicating relative enrichment of light elements and relative depletion of heavy elements, suggesting that evaporation has a minor impact on the study area. The sample points for atmospheric precipitation and groundwater are primarily located near the evaporation line of surface water, and the groundwater sample points are situated between those of atmospheric precipitation and surface water, indicating that surface water is primarily recharged by atmospheric precipitation, while groundwater is recharged by both atmospheric precipitation and surface water.

Human Activities

Human activities such as mining, agricultural production, and domestic sewage discharge can affect the changes in hydrochemical components, mainly manifested in the production of higher levels of NO_3^-, Cl^-, and Na^+ from agricultural production and domestic sewage, while mining activities can generate more SO_4^{2-} [27, 48]. The relationship between NO_3^-/Na^+ and Cl^-/Na^+ is used to determine the impact of human activities on hydrochemical components. In the study area, the ratio ranges of Cl^-/Na^+ for surface water and groundwater are 0.39~0.71 and 0.34~1.06, respectively, and the ratio ranges of NO_3^-/Na^+ are 0.20~0.59 and 0.46~1.16, respectively, with all ratios greater than 0.1. The ratios of Cl^-/Na^+ and NO_3^-/Na^+ for mine water are 0.24 and 0.05, respectively. As shown in Fig. 9a, all surface water and groundwater samples fall in the upper right quadrant, while mine water is located in the lower right quadrant. This indicates that mine water in the study area is primarily controlled by rock weathering, while surface water and groundwater are jointly influenced by salt rock weathering and agricultural activities, with groundwater being more significantly affected by agricultural activities.

Further analysis of the impact of different human activities on the hydrochemical composition can be conducted through the relationship between SO_4^{2-}/Ca^{2+} and NO_3^-/Ca^{2+}. Typically, the SO_4^{2-}/Ca^{2+} ratio is greater than the NO_3^-/Ca^{2+} ratio in mining activity areas, while the opposite is true in areas of human life and agricultural production [27]. In the study area, the ratio ranges of SO_4^{2-}/Ca^{2+} and NO_3^-/Ca^{2+} in surface water are 0.16~2.15 and 0.01~0.05, respectively, with the SO_4^{2-}/Ca^{2+} ratio significantly higher than the NO_3^-/Ca^{2+} ratio. For groundwater, the ratio ranges of SO_4^{2-}/Ca^{2+} and NO_3^-/Ca^{2+} are 0.24~0.37 and 0.04~0.15, respectively, with little

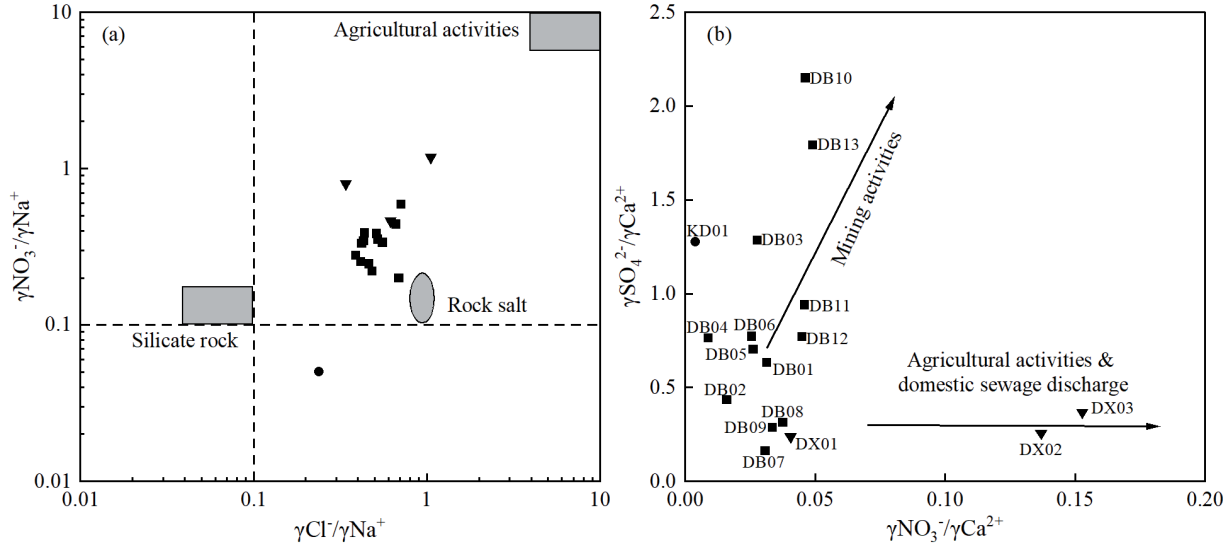

Fig. 9. NO_3^-/Na^+ versus Cl^-/Na^+ diagram (a) and SO_4^{2-}/Ca^{2+} versus NO_3^-/Ca^{2+} (b) diagram.

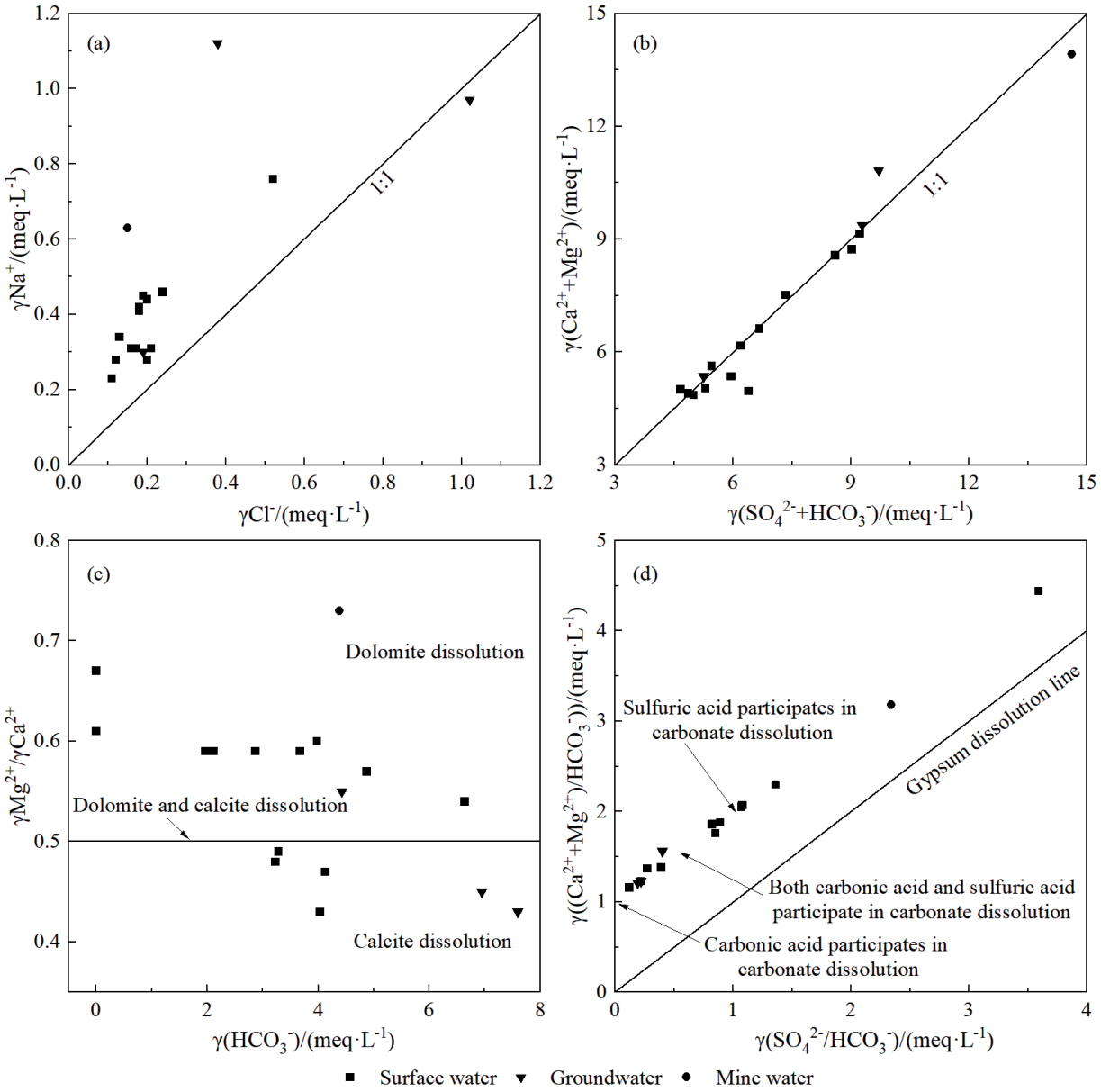

Fig. 10. The major ions combination relationship of surface water, groundwater, and mine water.

difference between the two ratios. As shown in Fig. 9b, surface water and mine water are primarily distributed in the upper left quadrant, indicating that surface water is significantly influenced by mining activities. This is related to the increase in SO_4^{2-} ions in surface water due to the leaching of mine waste (DB01, DB02, DB04) and the addition of chemical agents for treatment (DB10, DB13) in the mining area. Groundwater, on the other hand, is distributed in the lower right quadrant, suggesting that it is mainly affected by agricultural activities and domestic sewage discharge. However, the hydrochemical type of groundwater in the downstream section of the Luo River changes from HCO_3-Ca·Mg (DX02) to HCO_3·SO_4-Ca·Mg (DX03), with a notable increase in SO_4^{2-}, indicating that mining activities have had a certain impact on the groundwater.

Sources of Major Ions

The sources of Na^+ and Cl^- in water bodies can be reflected by the equivalent concentration ratio. The Na^+/Cl^- ratio in atmospheric precipitation is approximately 0.86; when $Na^+/Cl^- = 1$, it is mainly due to the dissolution of rock salt; when $Na^+/Cl^- > 1$, there may be silicate dissolution or other sources [49]. According to the ratio of Na^+ and Cl^- in Fig. 10a, most water sampling points fall above the 1:1 line, indicating that in addition to atmospheric precipitation and rock salt dissolution, the excess Na^+ mainly comes from the dissolution of sodium-containing silicates and the contribution of cation exchange [28]. Judging from the distribution of sample points, surface water sample points are relatively concentrated, while groundwater sample points are relatively dispersed. Sample points DB03, DX02,

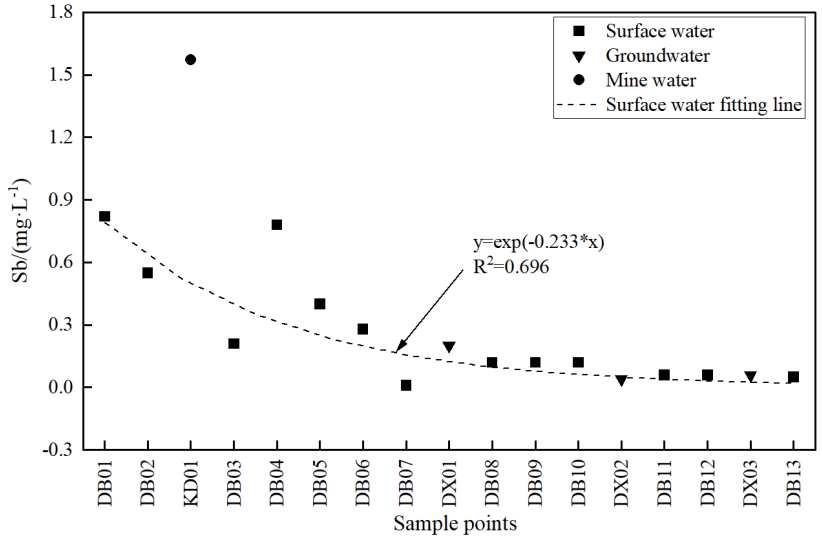

Fig. 11. Variation of antimony ion concentration along different water bodies in the study area.

and DX03 show abnormalities. DB03 is a wastewater treatment plant, which may be related to the increase in Cl^- content caused by the addition of treatment agent $FeCl_3$. DX02 and DX03 are located in residential areas, and previous analysis found that the Cl^- content in groundwater is greatly affected by human activities.

The sources of Ca^{2+} and Mg^{2+} can be judged based on the ion ratio relationship between $Ca^{2+}+Mg^{2+}$ and $SO_4^{2-}+HCO_3^-$ [50, 51]. Most sample points in Fig. 10b are distributed along the 1:1 line, indicating that Ca^{2+} and Mg^{2+} in the water bodies in the study area mainly come from the weathering of carbonate rocks and the dissolution of gypsum. However, the sample points of mine water and some surface water are located below the 1:1 line, suggesting that Ca^{2+} and Mg^{2+} in this part of the water may come from the dissolution of silicate minerals.

In the carbonate dissolution area, the ratio of Mg^{2+}/Ca^{2+} to HCO_3^- can be used to determine the contribution of calcite and dolomite dissolution in water bodies [52]. In the study area, the Mg^{2+}/Ca^{2+} ratio of surface water ranges from 0.43 to 0.67, with a mean value of 0.56; the Mg^{2+}/Ca^{2+} ratio of groundwater ranges from 0.43 to 0.55, with a mean value of 0.48; and the Mg^{2+}/Ca^{2+} ratio of mine water is 0.73. In Fig. 10c, the water sample points falling within the dolomite and calcite dissolution control areas account for 64.71% and 35.29% respectively, indicating that dolomite dissolution is the main source of Ca^{2+} and Mg^{2+} in the carbonate dissolution area, followed by calcite dissolution.

In nature, the main acids involved in the dissolution process of carbonate rocks are carbonic acid and sulfuric acid. Carbonic acid mainly comes from CO_2 in the atmosphere and soil, while sulfuric acid comes from acid rain or the oxidation of sulfur-bearing minerals. The dissolution characteristics of carbonate rocks are often analyzed using the relationship between $(Ca^{2+}+Mg^{2+})/HCO_3^-$ and SO_4^{2-}/HCO_3^-. When $(Ca^{2+}+Mg^{2+})/HCO_3^-=1$ and $SO_4^{2-}/HCO_3^-=0$, only carbonic acid is involved in the dissolution of carbonate rocks; when $(Ca^{2+}+Mg^{2+})/HCO_3^-=2$ and $SO_4^{2-}/HCO_3^-=1$, only sulfuric acid is involved [27, 49]. In Fig. 10d, all sample points are distributed parallel to the gypsum line and above the line where $(Ca^{2+}+Mg^{2+})/HCO_3^-=1$, indicating that both carbonic acid and sulfuric acid participate in the dissolution of carbonate rocks. However, mine water and some surface water are dominated by sulfuric acid in the dissolution of carbonate rocks. Given the large amount of sulfide tailings in the water environment of the study area, it is suggested that this portion of SO_4^{2-} mainly comes from the oxidation of stibnite and pyrite, with the reaction equations as follows [3]:

$$Sb_2S_3 + 6O_2 + 3H_2O \rightarrow Sb_2O_3 + 6H^+ + 3SO_4^{2-} \quad (1)$$

$$2FeS_2 + 7O_2 + 2H_2O \rightarrow 2FeSO_4 + 4H^+ + 2SO_4^{2-} \quad (2)$$

The concentration of antimony in the surface water in the study area ranges from 0.01 to 0.82 mg/L (average of 0.28 mg/L), with the concentration in the Gaolinggou antimony mining area (DB01-DB06) ranging from 0.21 to 0.82 mg/L (average of 0.51 mg/L) and that in the mainstream of the Luohe River (DB07-DB13) ranging from 0.01 to 0.12 mg/L (average of 0.08 mg/L). The average concentration in the Gaolinggou antimony mining area is 6.4 times that of the Luohe River mainstream. The concentration of antimony in groundwater ranges from 0.04 to 0.20 mg/L (average of 0.10 mg/L), while the concentration of antimony in mine water is 1.57 mg/L. Fig. 11 shows that the highest concentration of antimony is found in mine water KD01, while the lowest is in surface water DB07, which is a water sample taken before Gaolinggou flows into the Luohe River mainstream and represents water unaffected by antimony mining activities. The fitted line for antimony concentration in surface water in the

study area is y= exp(-0.233*x) (R^2=0.696), indicating that the concentration gradually decreases with changes in surface runoff, which is related to the self-purification capacity of water and human purification treatments. The antimony concentration in groundwater also shows a gradually decreasing trend, and most of the antimony concentrations in groundwater are located near the fitted line of antimony concentrations in surface water, suggesting that the antimony concentration in groundwater is influenced by surface water. Additionally, hydrogen and oxygen isotope analysis shows that surface water is mainly replenished by atmospheric precipitation, while groundwater is replenished by both atmospheric precipitation and surface water. Comprehensive analysis indicates that the antimony in surface water in the study area is mainly affected by mining activities in the Gaolinggou antimony mining area, while the antimony in groundwater is related to the lateral recharge of surface water.

Conclusions

1. The average pH value of surface water in the study area is 7.21, showing neutrality overall and acidity in some areas. The average TH is 314.69 mg/L, and the average TDS is 384.38 mg/L. The dominant cations are Ca^{2+} and Mg^{2+}, while the dominant anions are HCO_3^- and SO_4^{2-}. The hydrochemical types include HCO_3·SO_4-Ca·Mg, SO_4·HCO_3-Ca·Mg, HCO_3-Ca·Mg, and SO_4-Ca·Mg, with frequent spatial variations. For groundwater, the average pH is 7.52, and the average TH and TDS are 426.67 mg/L and 504.67 mg/L, respectively, slightly higher than those of the surface water. The dominant cations and anions are Ca^{2+} and HCO_3^-, respectively, and the hydrochemical types are HCO_3-Ca·Mg and HCO_3·SO_4-Ca·Mg. The mine water has a pH value of 8.03, indicating weak alkalinity, with the highest TDS content. It is enriched with SO_4^{2-}, Ca^{2+}, and Mg^{2+}, and its hydrochemical type is SO_4·HCO_3-Ca·Mg.

2. The hydrochemical characteristics of the study area are primarily controlled by rock weathering, manifested as the combined effects of weathering and dissolution of carbonate rocks and silicate rocks, with carbonate rock weathering as the dominant process. Positive cation exchange occurs in the water bodies, with the intensity of this process being greater in surface water than in groundwater. Surface water is primarily replenished by atmospheric precipitation, while groundwater is replenished by both atmospheric precipitation and surface water. Surface water is significantly impacted by mining activities, while groundwater is mainly affected by agricultural activities and domestic sewage discharge. However, mining activities have also had a certain impact on groundwater in the downstream area of the Luo River.

3. In addition to atmospheric precipitation and halite dissolution, the excess Na^+ in water bodies mainly originates from the dissolution of sodium-bearing silicates and cation exchange. Ca^{2+} and Mg^{2+} are primarily sourced from the weathering of carbonate rocks and the dissolution of gypsum, with contributions from the dissolution of silicate minerals. Dolomite dissolution is the primary source of Ca^{2+} and Mg^{2+} in carbonate rock dissolution areas, followed by calcite dissolution. Both carbonic acid and sulfuric acid participate in the dissolution of carbonate rocks. SO_4^{2-} and Cl^- are significantly influenced by mining activities. The antimony in surface water is mainly affected by mining activities in the Gaolinggou antimony mining area, while the antimony in groundwater is related to lateral recharge from surface water.

Data Availability Statement

The data described in the manuscript can be obtained from the corresponding author upon reasonable request.

Acknowledgments

This work was supported by the Geological survey project of China Geological Survey (DD20230481, DD20242461).

Conflict of Interest

The authors declare no conflict of interest.

References

1. BOREIKO C.J., ROSSMAN T.G. Antimony and its compounds: Health impacts related to pulmonary toxicity, cancer, and genotoxicity. Toxicology and Applied Pharmacology, **403** (1), 115156, **2020**.
2. LIU X.Y., WANG Y.Y., XIANG H.R., WU J.H., YAN X., ZHANG W.C., LIN Z., CHAI L.Y. Unveiling the crucial role of iron mineral phase transformation in antimony(V) elimination from natural water. Eco-Environment & Health, **2** (3), 176, **2023**.
3. FU X.X., XIE X.J., CHARLET L., HE J. A review on distribution, biogeochemistry of antimony in water and its environmental risk. Journal of Hydrology, **625**, 130043, **2023**.
4. CHEN L.Y., REN B.Z., DENG X.P., YIN W., XIE Q., CAI Z.Q. Potential toxic heavy metals in village rainwater runoff of antimony mining area, China: Distribution, pollution sources, and risk assessment. Science of The Total Environment, **920**, 170702, **2024**.
5. SHANAWANY S.E., FODA N., HASHAD D.I., SALAMA N., SOBH Z. The potential DNA toxic changes among workers exposed to antimony trioxide. Environmental science and pollution research international, **24** (13), 12455, **2017**.
6. LUO J.L., ZHANG C.P., YANG Z.Y., LIU F.Z., LUO H. Influence of dissolved organic matter on antimony speciation and distribution in mining polluted reservoir.

Acta Scientiae Circumstantiae, **43** (3), 226, **2023** [In Chinese].
7. HE M.C., WANG X.Q., WU F.C., FU Z.Y. Antimony Pollution in China. Science of the Total Environment, **421/422**, 41, **2012**.
8. HERATH I., VITHANAGE M., BUNDSCHUH J. Antimony as a global dilemma: Geochemistry, mobility, fate and transport. Environmental Pollution, **223** (16), 545, **2017**.
9. PIERART A., SHAHID M., SÉJALON-DELMAS N., DUMAT C. Antimony bioavailability: Knowledge and research perspectives for sustainable agricultures. Journal of Hazardous Materials, **289**, 219, **2015**.
10. GUO Q.H., PLANER-FRIEDRICH B., LUO L., LIU M.L., WU G., LI Y.M., ZHAO Q. Speciation of antimony in representative sulfidic hot springs in the YST Geothermal Province (China) and its immobilization by spring sediments. Environmental Pollution, **266** (Pt 1), 115221, **2020**.
11. LI X., GUO HQ.H., ZHAO Q. Dissolution of stibnite and the morphological distribution of antimony in its products under different aqueous conditions. Earth Science, **49** (11), 4022, **2024** [In Chinese].
12. NIEDZIELSKI P., SIEPAK J., SIEPAK M. Total Content of Arsenic, Antimony and Selenium in Groundwater Samples from Western Poland. Polish Journal of Environmental Studies, **10** (5), 347, **2001**.
13. QUINO-LIMA I., RAMOS-RAMOS O., ORMACHEA-MUÑOZ M., QUINTANILLA-AGUIRRE J., DUWIG C., MAITY J.P., SRACEK O., BHATTACHARYA P. Spatial dependency of arsenic, antimony, boron and other trace elements in the shallow groundwater systems of the Lower Katari Basin, Bolivian Altiplano. Science of the Total Environment, **719**, 137505, **2020**.
14. SEN I.S., PEUCKER-EHRENBRINK B. Anthropogenic Disturbance of Element Cycles at the Earth's Surface. Environmental Science & Technology, **46** (16), 8601, **2012**.
15. CHU J.W., HU X.Y., KONG L.H., WANG N.N., ZHANG S.H., HE M.C., OUYANG W., LIU X.T., LIN C.Y. Dynamic flow and pollution of antimony from polyethylene terephthalate (PET) fibers in China. Science of the Total Environment, **771**, 144643, **2021**.
16. TELFORD K., MAHER W., KRIKOWA F., FOSTER S., ELLWOOD M.J., ASHLEY P.M., LOCKWOOD P.V., WILSON S.C. Bioaccumulation of antimony and arsenic in a highly contaminated stream adjacent to the Hillgrove Mine, NSW, Australia. Environmental Chemistry, **6** (2), 133, **2009**.
17. BABAYAN G.H., SAKOYAN G.A., SAHAKYAN G.A. Assessing the quality of water from surface sources of drinking water supply to towns of south Armenia. Electronic Journal of Natural Sciences, **28** (1), 3, **2017**.
18. KEYVN Z., NEJAT Z., ESMAEIL S., JALIL M., SIAVASH G., HAMED A., FARYAD K. Arsenic, lead and antimony contamination of the Sefidrud sub-basin (Kurdistan province): An indication for the high incidence of gastric and esophagus cancers in Northwest Iran. Groundwater for Sustainable Development, **23**, 100982, **2023**.
19. JEONG C.H. Case Study of Hydrochemical Contamination by Antimony Waste Disposal in Korea. The Journal of Engineering Geology, **18** (4), 471, **2008**.
20. REN W., RAN Y.Y., MOU Y.W., CUI Y.X., SUN B.Y., YU L., WAN D.X., HU D.Y., ZHAO P. Pollution characteristics and risk assessment of antimony and arsenic in a typical abandoned antimony smelter. Environmental Geochemistry and Health, **45** (7), 5467, **2023**.
21. CHEN L.Y., REN B.Z., DENG X.P., YIN W., XIE Q., CAI Z.Q. Potential toxic heavy metals in village rainwater runoff of antimony mining area, China: Distribution, pollution sources, and risk assessment. Science of The Total Environment, **920**, 170702, **2024**.
22. HAO C.M., LIU M., PENG Y.G., WEI Z.B. Comparison of Antimony Sources and Hydrogeochemical Processes in Shallow and Deep Groundwater Near the Xikuangshan Mine, Hunan Province, China. Mine Water And The Environment, **41** (1), 194, **2022**.
23. LIU L.H., TULCAN R.X.S., HE M.C., OUYANG W., ZHANG Q.W., YARLEQUE C.M.H., CHICAIZA-ORTIZ C. Antimony pollution threatens soils and riverine habitats across China: An analysis of antimony concentrations, changes, and risks. Critical Reviews in Environmental Science and Technology, 1, **2023**.
24. LI C., RAN Y.Y., WU P., LIU P., YANG B.Y., GU X.Y., ZHAO P., LIU S.R., SONG L., LIU Y.H., NIN Z.P., SUN J., LIU C.S. Antimony and arsenic migration in a heterogeneous subsurface at an abandoned antimony smelter under rainfall. Journal of Hazardous Materials, **470**, 134156, **2024**.
25. LAN J.M., JIANG T., MEI J.H., TANG H., HUANG W.Z. Characterization and causes of interannual variation of antimony contamination in groundwater of a typical antimony mining area. Hydrogeology & Engineering Geology, **50** (5), 192, **2023** [In Chinese].
26. WANG J., LUO Z.H., CHEN Z.H., WANG T., HUANG H., XIANG C.J., SUN B.T., WANG Y. Characteristics and controlling factors of water chemistry in mapping lead-zinc mine area, Northeastern Yunnan, China. Environmental Chemistry, **37** (6), 1421, **2018** [In Chinese].
27. LIU H., KANG B., GUAN Z.T., SONG Y., CHAI Y.L. Hydrochemical Characteristics and Control Factors of Surface Water and Groundwater in Huainan Coal Mine Area. Environmental Science, **44** (11), 6038, **2023** [In Chinese].
28. BARZEGAR R., MOGHADDAM A.A., TZIRITIS E., FAKHRI M.S., SOLTANI S. Identification of hydrogeochemical processes and pollution sources of groundwater resources in the Marand plain, northwest of Iran. Environmental Earth Sciences, **76** (7), 296, **2017**.
29. WANG X.L., AJI D., TUOHETI S. Analysis of the Hydrochemical Characteristics and Genesis of Bosten Lake, China. Sustainability, **15** (5), 4139, **2023**.
30. YAN Z.X., FENG M.Q. Hydrochemical characteristics and driving factors of surface water in the mining area of Changhe River Basin. Environmental Chemistry, **41** (2), 632, **2022** [In Chinese].
31. SUN H.Y., WANG C.S., WEI X.F., ZHU X.Y., HUANG X.K. Hydrochemical characteristics and driving factors in the water of the Bayingaole Basin, Southern Great Xing'an Range. Environmental Chemistry, **39** (9), 2507, **2020** [In Chinese].
32. LI P.Y., TIAN R., LIU R. Solute Geochemistry and Multivariate Analysis of Water Quality in the Guohua Phosphorite Mine, Guizhou Province, China. Expo Health, **11**, 81, **2019**.
33. FARID I., TRABELSI R., ZOUARI K., ABID K., AYACHI M. Hydrogeochemical processes affecting groundwater in an irrigated land in Central Tunisia. Environmental Earth Sciences, **68** (5), 1215, **2013**.
34. GIBBS R.J. Mechanisms controlling world water chemistry. Science, **170** (3962), 1088, **1970**.
35. MARANDI M., SHAND P. Groundwater chemistry and

the Gibbs Diagram. Applied Geochemistry, **97** (1), 209, **2018**.
36. PIPER A.M. A graphic procedure in the geochemical interpretation of water-analyses. Eos Transactions American Geophysical Union, **25** (6), 914, **1944**.
37. WANG Q.L. A Preliminary Discussion On The Genesis Of Antimony Deposits In Northern Shangxian-Danfeng Area. Mineral Deposit, **3** (4), 45, **1984** [In Chinese].
38. ZHANG Z.W., ZHANG J.J., HUANG H.M., ZHANG Z.S. The Characteristics of Sb Deposits and Its Structure Control Function about Northern of Antimony Mineral Belt in East Qinling. Bulletin of Mineralogy, Petrology and Geochemistry, **26** (2), 185, **2007** [In Chinese].
39. WANG X.X. Main ore controlling factors and genesis of Gaolinggou-Danfeng caiao antimony ore belt in Shang County. Northwestern Geology, (5), 28, **1985** [In Chinese].
40. GAILLARDET J., DUPRE B., LOUVAT P., ALLEGRE C.J. Global silicate weathering and CO_2 consumption rates deduced from the chemistry of large rivers. Chemical Geology, **159**, 3, **1999**.
41. GAN Y.Q., ZHAO K., DENG Y.M., LIANG X., MA T., WANG Y.X. Groundwater flow and hydrogeochemical evolution in the Jianghan Plain, central China. Hydrogeology Journal, **26** (5), 1609, **2018**.
42. LI P.Y., WU J.H., QIAN H., ZHANG Y.T., YANG N., JING L.J., YU P.Y. Hydrogeochemical Characterization of Groundwater in and Around a Wastewater Irrigated Forest in the Southeastern Edge of the Tengger Desert, Northwest China. Water Quality, Exposure and Health, **8** (3), 331, **2016**.
43. SCHOELLER H. Qualitative evaluation of groundwater resources. In Methods and techniques of groundwater investigation and development. Water Research, Series-33. UNESCO, Delft, 54, **1965**.
44. CHARFI S., ZOUARI K., FEKI S., MAMI E. Study of variation in groundwater quality in a coastal aquifer in north-eastern Tunisia using multivariate factor analysis. Quaternary International, **302**, 199, **2013**.
45. JIN Y., JIANG Y.H., DONG X.Z., YANG G.Q., LIU H.Y., LEI C.Z., ZHOU Q.P., ZHANG H., MEI S.J., YANG H., LV J.S., LI Y. Chemical characteristics and eco-environmental effect of groundwater in Ningbo Plain, Zhejiang Province. Geology In China, **49** (5), 1527, **2022** [In Chinese].
46. CRAIG H. Isotopic Variations in Meteoric Waters. Science, **133** (3465), 1701, **1961**.
47. ZHANG S.C. Characteristics of hydrogen-oxygen isotope compositions of contemporarily atmospheric sedimentation in Shaanxi province. Geology of Shaanxi, **7** (2), 57, **1989** [In Chinese].
48. TU C.L., YIN L.H., HE C.Z., CUN D.X., MA Y.Q., LINGHU C.W. Hydrochemical Composition Characteristics and Control Factors of Xiaohuangni River Basin in the Upper Pearl River. Environmental Science, **43** (4), 1885, **2022** [In Chinese].
49. WANG P., JIN M.G., LU D.C. Hydrogeochemistry Characteristics and Formation Mechanismof Shallow Groundwater in Yongcheng City, Henan Province. Earth Science, **45** (6), 2232, **2020** [In Chinese].
50. SUN Q.F., YANG K., SUN Z.A., JIA L.G., TIAN H., GUO X.D., LI X.G., ZHU W. Characteristics of groundwater quality in Changchun New Area and its evaluation on ecological health. Geology In China, **49** (3), 834, **2022** [In Chinese].
51. PU J.B., YUAN D.X., XIAO Q., ZHAO H.P. Hydrogeochemical characteristics in karst subterranean streams: a case history from Chongqing, China. Carbonates And Evaporites, (3), 30, **2015**.
52. ABDELKADER R., LARBI D., RIHAB H., FETHI B., CHEMSEDDINE F., AZZEDINE H. Geochemical characterization of groundwater from shallow aquifer surrounding Fetzara Lake N.E.Algeria. Arabian Journal of Geosciences, **5** (1), 1, **2012.**